


The survival and proliferation of osteosarcoma cells are dependent on the mitochondrial BIG3-PHB2 complex formation

Shunichi Toki^{1,2} | Tetsuro Yoshimaru¹ | Yosuke Matsushita¹ | Hitoshi Aihara¹ | Masaya Ono³ | Koichi Tsuneyama⁴ | Koichi Sairyō² | Toyomasa Katagiri¹ 

¹Division of Genome Medicine, Advanced Institute of Medical Sciences, Tokushima University, Tokushima, Japan

²Department of Orthopedics, Institute of Biomedical Sciences, Tokushima University Graduate School, Tokushima, Japan

³Department of Proteomics, National Cancer Center Research Institute, Tokyo, Japan

⁴Department of Pathology and Laboratory Medicine, Institute of Biomedical Sciences, Tokushima University Graduate School, Tokushima, Japan

Correspondence

Toyomasa Katagiri, Division of Genome Medicine, Advanced Institute of Medical Sciences, Tokushima University, 3-18-15, Kuramoto-cho, Tokushima 770-8503, Japan.
Email: tkatagi@genome.tokushima-u.ac.jp

Funding information

Ministry of Education, Culture, Sports, Science and Technology, Grant/Award Number: JP16H05153, JP17H06419, JP20H00543 and JP18K07200; Japan Agency for Medical Research and Development, Grant/Award Number: 19191248

Abstract

Previous studies reported the critical role of the brefeldin A-inhibited guanine nucleotide exchange protein 3-prohibitin 2 (BIG3-PHB2) complex in modulating estrogen signaling activation in breast cancer cells, yet its pathophysiological roles in osteosarcoma (OS) cells remain elusive. Here, we report a novel function of BIG3-PHB2 in OS malignancy. BIG3-PHB2 complexes were localized mainly in mitochondria in OS cells, unlike in estrogen-dependent breast cancer cells. Depletion of endogenous BIG3 expression by small interfering RNA (siRNA) treatment led to significant inhibition of OS cell growth. Disruption of BIG3-PHB2 complex formation by treatment with specific peptide inhibitor also resulted in significant dose-dependent suppression of OS cell growth, migration, and invasion resulting from G2/M-phase arrest and in PARP cleavage, ultimately leading to PARP-1/apoptosis-inducing factor (AIF) pathway activation-dependent apoptosis in OS cells. Subsequent proteomic and bioinformatic pathway analyses revealed that disruption of the BIG3-PHB2 complex might lead to downregulation of inner mitochondrial membrane protein complex activity. Our findings indicate that the mitochondrial BIG3-PHB2 complex might regulate PARP-1/AIF pathway-dependent apoptosis during OS cell proliferation and progression and that disruption of this complex may be a promising therapeutic strategy for OS.

KEYWORDS

BIG3, mitochondria, osteosarcoma, peptide inhibitor, PHB2

1 | INTRODUCTION

Osteosarcoma (OS) is the most common primary malignant bone tumor that is mainly developing during childhood and adolescence.¹ Although the 5-year survival rate of patients with OS without distant metastasis is 76%,¹ those of patients with metastases at initial diagnosis and relapsed

or refractory disease remain poor—45%¹ and 13% to 40%,² respectively. The combination of surgical wide resection and adjuvant chemotherapy using multiple agents, such as doxorubicin, cisplatin, high-dose methotrexate, and ifosfamide, is the standard first-line treatment approach for high-grade OS either with or without metastases.³ For relapsed or refractory disease, although several agents and regimens, including molecular

This is an open access article under the terms of the Creative Commons Attribution-NonCommercial License, which permits use, distribution and reproduction in any medium, provided the original work is properly cited and is not used for commercial purposes.

© 2021 The Authors. *Cancer Science* published by John Wiley & Sons Australia, Ltd on behalf of Japanese Cancer Association.

targeted therapies and immunotherapy, have been studied, an effective systematic therapy has not yet been established for OS in the last three decades.⁴ The most urgent issue is to develop novel therapeutic agents for patients with either advanced or relapsed OS.

Recent genome-wide next-generation sequencing studies have identified several frequently mutated genes and tumor-specific genome alterations mediating OS tumorigenesis⁵ that differ from those of other sarcomas, which are categorized by specific chromosomal translocations. These studies have shown important genomic alteration events in OS, including *TP53* and *RB1* gene mutation; *MYC*, *CCNE1*, and *CDK4* gene amplification; and *BRCA1*, *BRCA2*, and *PTEN* gene deletion.⁵ However, the identification of these potential driver genes involved in OS tumorigenesis and progression have failed to provide important insight that can help to improve OS treatment.

We demonstrated that brefeldin A-inhibited guanine nucleotide exchange protein 3 (BIG3) is frequently upregulated in the vast majority of estrogen receptor alpha (ER α)-positive breast cancer specimens and that high BIG3 expression levels are strongly associated with poor prognosis in patients with ER α -positive breast cancers.^{6,7} Moreover, BIG3 acts as a critical modulator of estrogen signaling in breast cancer cells by inhibiting the tumor-suppressive activity of prohibitin 2 (PHB2).⁶ An antitumor agent constituted by a specific peptide inhibitor targeting the BIG3-PHB2 interaction, ie, stapled ER α activity regulator synthetic peptide (stERAP), that exploits the tumor-suppressive activity of PHB2 has been developed.⁷⁻¹¹ By contrast, analysis of RNA-seq data in public databases revealed high expression of the BIG3 (gene name: *ARFGEF3*) in various cancers, including OS, but did not elucidate the functional roles of BIG3 in other cancers, especially OS.

In this study, we focused on understanding the pathophysiological role of the BIG3-PHB2 complex in OS tumorigenesis and progression. Moreover, unexpectedly, we provided the first demonstration that the BIG3-PHB2 complex is localized in mitochondria in OS cells and that stERAP has potential as a therapeutic drug targeting OS cells.

2 | MATERIALS AND METHODS

2.1 | Cell lines

The human OS cell lines MG-63 and HOS were obtained from the Japanese Collection of Research Bioresources Cell Bank (JCRB). Saos-2 and U-2OS cells were obtained from Riken BRC and The European Collection of Authenticated Cell Cultures (ECACC), respectively. The human osteoblast cell line HOB was purchased from Takara Bio, Inc. All cell lines were cultured under the corresponding depositor's recommendations. The cell line stocks used in this study had been properly stored in liquid nitrogen. The morphologies of these cells were monitored by microscopy, and maintenance of their morphology was confirmed by comparison of images with the original morphological images. No *Mycoplasma* contamination was

detected in any of the cultures using a MycoAlert™ Mycoplasma Detection kit (Lonza).

2.2 | stERAP

stERAP, which was designed to specifically inhibit the BIG3-PHB2 interaction, was synthesized by Polypeptide Laboratories (San Diego, USA) in accordance with a previous report.¹¹

2.3 | Quantitative reverse-transcription PCR (qRT-PCR)

Total RNA extraction and subsequent complementary DNA synthesis were performed as described previously.⁷ Then, expression of the *PARP1* and *ACTB* genes was evaluated by qRT-PCR using a 7500 Real Time PCR System (Applied Biosystems) and Power SYBR Green PCR Master Mix (Applied Biosystems) as described previously.⁷ The mRNA content of the *PARP1* gene was normalized to the *ACTB* mRNA content. The data are presented as the mean \pm standard deviation (SD) of three or six independent experiments. The primers used were as follows: 5'-ACTGAGAAATCACGCACTGT-3'; *PARP1*, 5'-CCCAGGGTCTTCGGATAG-3' and 5'-AGCGTGCTTCAGTTCATACA-3'; and *ACTB*, 5'-ATTGCCGACAGGATGCAG-3' and 5'-CTCAGGAGGAGCAATGATCTT-3'.

2.4 | Antibodies and immunoblot analysis

Cell lysis, SDS-PAGE and immunoblot analysis were performed as described previously.⁸ Membranes were incubated with antibodies against the following proteins: BIG3 (diluted 1:250),⁶ PHB2 (Abcam #ab71970, diluted 1:1000), β -actin (clone AC-15, Sigma-Aldrich #A1978, diluted 1:5000), PARP (CST #9542, diluted 1:500), and apoptosis-inducing factor (AIF) (clone E-1, Santa Cruz Biotechnology #sc-13116, diluted 1:200). After incubation with HRP-conjugated secondary antibodies (anti-mouse IgG-HRP, diluted 1:5000; anti-rat IgG-HRP, diluted 1:5000; anti-rabbit IgG-HRP, diluted 1:1000 [Santa Cruz Biotechnology]) for 1 hour, the blots were developed with an enhanced chemiluminescence system (GE Healthcare) and scanned using an Image Reader LAS-3000 Mini (Fujifilm).

2.5 | Analysis of public database of RNA expression and prognosis in OS patients

Gene expression data from 39 patients with OS without metastases at diagnosis from the GSE21257 dataset were used for this analysis. The mRNA expression data were calculated using GEO2R of NCBI, and patient clinical data, including overall survival and metastasis at diagnosis, were also referred to a previously report.¹²

2.6 | Gene silencing by small interfering RNAs (siRNAs)

The sequences targeting *BIG3* (siBIG3) and enhanced green fluorescent protein (EGFP) (siEGFP) were as follows: siBIG3, 5'-GAUCGCUUCUCUGCCACACTT-3'; siEGFP, 5'-GCAGCACGACUUCUUCAG-3'. Human OS MG-63 cells (1.0×10^4) were transfected with 10 nM of each siRNA using Lipofectamine RNAiMAX (Invitrogen) in OptiMEM (Invitrogen) as described previously.⁸ The first transfection was performed immediately after cell seeding, and the second transfection was performed 4 days later. Time course analysis of both siRNA-transfected cell lines was carried out for 7 days.

2.7 | Immunocytochemistry

MG-63 cells (2.0×10^3) were seeded in eight-well chambers (Nunc Lab-Tek II Chamber Slide System, Thermo Fisher Scientific) and incubated at 37 °C. Cells were then treated with stERAP for 24 or 48 hours. Staining was conducted with previously described procedures,⁸ using antibodies against BIG3 (diluted 1:500),¹¹ PHB2 (clone 7F8E3, MABC953, diluted 1:500), and PARP (clone 46D11, CST #9532, diluted 1:500), and with 500 nM MitoTracker (MT) Red CMXRos (Invitrogen) incubation for 30 minutes at 37 °C before fixation. Nuclei were counterstained with 4',6'-diamidino-2'-phenylindole dihydrochloride (DAPI). Fluorescent images were obtained under FV3000 confocal microscopy (Olympus).

2.8 | Phalloidin staining

MG-63, HOS, and Saos-2 cells (1.0×10^4 /well) were treated with 1 μM stERAP under the appropriate media in a slide chamber. Subsequently, cells were fixed and stained with an Alexa Fluor™ 488 Phalloidin (ThermoFisher), and following procedures were performed as described previously.^{7,8}

2.9 | Cell proliferation assay

Proliferation assays of MG-63, Saos-2, U-2 OS, and HOS were performed using a hemocytometer and Cell Counting Kit-8 (CCK-8) (Dojindo) as described previously.⁸ The data are presented as the mean \pm standard error (SE) of three or more independent experiments. The half-maximal inhibitory concentration (IC_{50}) values of stERAP in each cell line were obtained from the sigmoidal inhibition curves fitted by regression analysis.¹¹

2.10 | Immunoprecipitation

Immunoprecipitation analyses were performed as described previously.⁸ Cells were lysed with lysis buffers including a protease

inhibitor cocktail (Complete, Roche) for analysis of BIG3 and PHB2 (50 mM Tris-HCl [pH 8.0], 150 mM NaCl, 0.1% NP-40, and 0.5% CHAPS) or for analysis of BIG3 and PARP (50 mM Tris-HCl [pH 7.5], 137 mM NaCl, 10% glycerol, 1 mM EDTA, 1 mM Na_3VO_4 , 20 mM β -glycerophosphate, 1 mM sodium pyrophosphate, 20 mM NaF, 0.5% dodecyl maltoside). The lysates were incubated with 5 μg of antibodies against BIG3 at 4 °C for 12 hours, and following procedures were performed as described previously.^{7,8}

2.11 | Cell migration and invasion assays

Wound healing assays with (for the invasion assay) or without (for the migration assay) Matrigel (BD) precoating were carried out to investigate the migration and invasion abilities of OS cells. Saos-2 cells (5.0×10^4) were seeded into 96-well plates and incubated at 37 °C for 24 hours. After microscopic confirmation of contact with the surface and an appropriate cell density, wounds were created on the assay plates by scratching with a specific instrument (WoundMaker, Essen Bioscience). For real-time quantitative live-cell imaging and analysis, cells were incubated in an IncuCyte® ZOOM System (Essen Bioscience) at 37 °C, and scanning was run for 96 hours.

2.12 | In vivo tumor growth inhibition by stERAP

HOS cell line was used for in vivo tumor growth inhibition assay because this cell line expresses BIG3 and PHB2 proteins and forms tumors easily in nude mouse.¹³ Each suspension (3×10^6 cells per mouse) of HOS cells was mixed with an equal volume of Matrigel (BD) and injected (200 μL total) into 6-week-old female BALB/c nude mice (Charles River Laboratories). The mice were housed in a pathogen-free isolation facility on a 12-hour light/dark cycle and were fed rodent chow and water ad libitum. The tumors developed over 6 days to a volume of ~ 100 mm³ (calculated as $1/2 \times [\text{width} \times \text{length}^2]$). Subsequently, the mice were randomized into two groups (five mice per group). Mice in one group received a weekly intravenous injection of 1 mg/kg stERAP, and mice in the other group received PBS as a control. Tumor volume was measured with calipers for 4 weeks; the animals were then sacrificed, and the tumors were excised. A portion of each tissue was fixed with 4% paraformaldehyde for histological examination, while the remaining tissue sample was frozen and stored at -80 °C for subsequent experiments. All animal experiments were performed in accordance with the guidelines of the animal facility at Tokushima University and approved by the institutional review board (T2019-113). For M30 cytodeath analysis, we stained 5-μm sections of paraffin-embedded tumors with an M30 monoclonal antibody (Peviva) to examine the M30 cytodeath protein expression in HOS xenograft tumors as described previously.¹⁴ The data represent the mean \pm SD of 10 different points.

2.13 | Mitochondrial isolation

Mitochondria were isolated from MG-63 cells using a human mitochondria isolation kit (Miltenyi Biotec, 130-094-532) according to the manufacturer's instructions.

2.14 | Statistical analyses

Unless mentioned otherwise, data are presented as the mean \pm SD of three or more samples, and two-tailed Welch's *t*-tests were run to compare means among samples using the SPSS software program (version 20; SPSS Statistics). Differences with $P < .05$ were considered statistically significant.

3 | RESULTS

3.1 | The OS cell growth is dependent on the mitochondrial BIG3 and PHB2 complex

Analysis of RNA-seq data for 934 human cancer cell lines from the Broad Institute Cancer Cell Line Encyclopedia (CCLE) in public databases showed that the expression of BIG3 in several OS cell lines was higher than that in other subtypes of malignant and intermediate mesenchymal bone tumors, including chondrosarcoma, Ewing sarcoma, and giant cell tumor of bone (Figure S1A). Notably, the expression of *BIG3* in tumors was upregulated compared with that in the corresponding adjacent normal tissues, as determined using total RNA in paired clinical samples in GEO (GSE126209) (Figure S1B).¹⁵ We verified that the expression of BIG3 and PHB2 was higher in all tested OS cell lines than in normal osteoblasts (ie, HOB cells) at the protein level (Figure 1A). Gene expression analysis based on public database shows that high expression of *BIG3* correlates with poor prognosis in patients with OS without metastases at diagnosis (GSE21257)¹² (Figure 1B). Subsequently, we investigated the subcellular localization of BIG3 and PHB2 in OS cells by immunocytochemical staining and unexpectedly found that endogenous BIG3 and PHB2 were colocalized with MT in MG-63 cells (Figure 1C), unlike the findings in ER-positive breast cancer cells reported previously.⁶ To confirm a potential role of *BIG3* in OS cell proliferation, we knocked down endogenous expression of *BIG3* by siRNA in MG-63 cells. Depletion of *BIG3* significantly suppressed the proliferation of MG-63 cells compared with siEGFP-transfected cells as the control (Figure 1D). Collectively, these findings suggest that BIG3 and PHB2 play an important role in mitochondria to support the growth of OS cells.

3.2 | Inhibition of mitochondrial BIG3-PHB2 complex formation suppresses the proliferation, migration, and invasion of OS cells

First, we confirmed by immunoprecipitation-immunoblot analyses that treatment with stERAP, a stapled ERAP inhibitor targeting the

BIG3-PHB2 interaction, inhibited the formation of the BIG3-PHB2 complex in the OS cell lines MG-63, Saos-2, and HOS (Figure 2A). Importantly, stERAP treatment resulted in significant suppression of cell proliferation in a dose-dependent manner (mean IC_{50} values: 241 nM in MG-63 cells, 99 nM in Saos-2 cells, 754 nM in U-2 OS cells, and 131 nM in HOS cells). However, stERAP treatment did not suppress cell proliferation of HOB cells (Figure S2) compared with OS cell lines (Figure 2B). In addition, we demonstrated that stERAP has no inhibitory effect on the proliferation of normal epithelial mammary gland cell line MCF-10A cells, which has no expression of BIG3.¹¹ Collectively, our findings suggest that the survival and proliferation of OS cells which have BIG3 and PHB2 expression are dependent on the mitochondrial BIG3-PHB2 complex. Moreover, real-time quantitative live-cell imaging analysis showed that stERAP suppressed the migration and invasion of Saos-2 cells in a dose-dependent manner (Figure 2C). Subsequently, we performed immunocytochemical staining to investigate the impact of stERAP treatment on the mitochondrial localization of the BIG3-PHB2 complex in OS cells by analyzing colocalization using the Pearson correlation coefficient. Interestingly, both BIG3 and PHB2 were still colocalized with MT in stERAP-treated cells (Pearson correlation coefficients: MT vs. BIG3, $R = 0.957$ in nontreated cells and $R = 0.961$ in stERAP-treated cells; MT vs. PHB2, $R = 0.663$ in nontreated cells and $R = 0.762$ in stERAP-treated cells) (Figure 2D and Figure S3). However, colocalization of BIG3 and PHB2 was reduced in stERAP-treated cells compared with nontreated cells (Pearson correlation coefficients: BIG3 vs. PHB2, $R = 0.875$ in nontreated cells and 0.652 in stERAP-treated cells) (Figure 2D and Figure S3). Collectively, these findings indicated that the BIG3-PHB2 complex remained localized in mitochondria in OS cells even though it was disrupted by stERAP treatment. These results suggest that formation of the mitochondrial BIG3-PHB2 complex plays a critical role in the proliferation and progression of OS cells.

3.3 | stERAP treatment leads to OS cell death

We noted that almost all MG-63 cells exhibited dose-dependent plasma membrane blebbing and apoptotic body formation, signs of apoptotic cell death, at 72 hours after treatment with stERAP (Figure S4A). To visualize such signs of apoptotic cell death, we attempted to do phalloidin staining to observe the actin cytoskeleton of MG-63, HOS, and Saos-2 cells as described previously.¹⁶ The result showed that almost all OS cells exhibited the time-dependent membrane blebbing and the formation of some apoptotic body-like small vesicles, signs of apoptotic cell death, at 24 hours after treatment with stERAP (Figure 3A and Figure S5A and S6A). We next assessed apoptosis by FITC-Annexin V staining. Figure 3B shows that after stERAP treatment, the percentage of late apoptotic cells was remarkably increased after 72 hours (no treatment, 24, 48, 72, and 96 hours: 1.9, 0.9, 6.2, 24.8, and 27.3%, respectively). In addition, we observed the same results in HOS and Saos-2 cells (Figure S5 and S6), suggesting that stERAP treatment can potentially induce

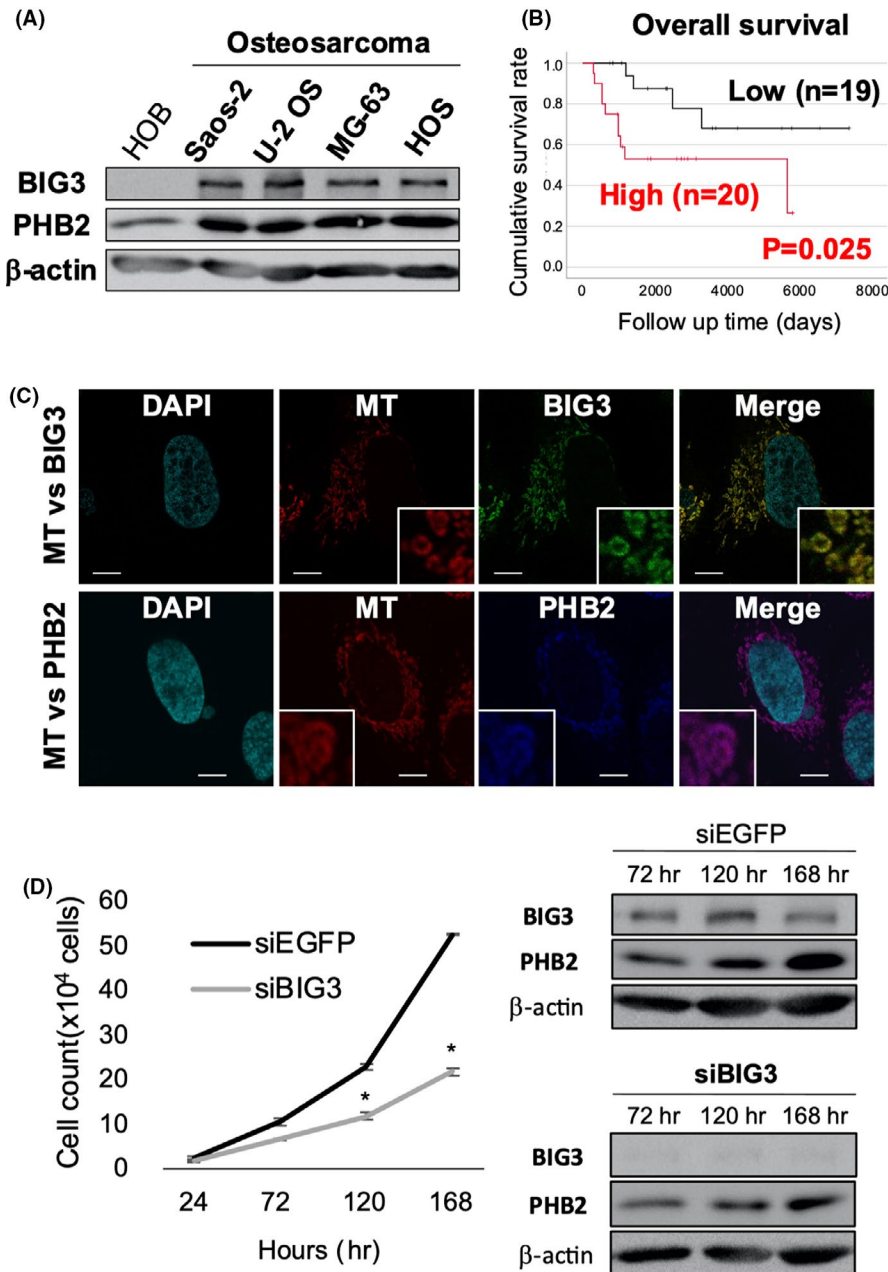


FIGURE 1 Upregulation of mitochondrial brefeldin A-inhibited guanine nucleotide exchange protein 3 (BIG3) is responsible for osteosarcoma (OS) cell growth. **A**, Expression of BIG3 and prohibitin 2 (PHB2) in the OS cell lines Saos-2, U-2 OS, MG-63, HOS, and the normal osteoblast line HOB at the protein level. **B**, Prognostic analysis (overall survival) of BIG3 expression in 39 OS patients without metastasis at diagnosis. Patients were grouped using median expression. The *P*-value was calculated by the log-rank test. **C**, Representative fluorescence confocal micrographs showing the mitochondrial localization of endogenous BIG3 and PHB2 in MG-63 cells. Nuclei were stained with DAPI (light blue) and mitochondria with MitoTracker (MT) Red CMXRos (red), BIG3 (green), and PHB2 (blue). Scale bar, 10 μ m. Two independent experiments were performed. **D**, (left) Knockdown of BIG3 expression by siRNA attenuated MG-63 cell proliferation. **P* < .05; (right) The expression of BIG3 knocked down by siRNA was validated by Western blotting. siEGFP was used as the negative control. β -actin was used as the quantitative control. Two independent experiments were performed.

apoptosis in OS cells. We next investigated the effect of stERAP on cell cycle arrest in OS cells by FACS analysis. The results show that the percentage of G2/M phase in MG-63 cells drastically increased 72 hours after stERAP treatment (Figure 3C). Similarly, the percentage of G2/M phase in HOS and Saos-2 cells drastically increased 48 hours after stERAP treatment (Figure S5B and S6B). Moreover, the percentages of cells in the sub-G1 phase in OS cells were gradually increased 72 hours after treatment with stERAP (MG-63; no treatment, 24, 48, 72, and 96 hours: 1.2, 3.2, 4.3, 11.0, and 19.5%, respectively). (Figure 3C; Figure S5C and S6C). Additionally, partial cleavage of the PARP protein was observed from approximately 72 to 96 hours after stERAP treatment in MG-63 cells (Figure 3D). Taken together, these results indicate that stERAP treatment causes G2/M-phase arrest, thereby finally inducing apoptosis in OS cells.

3.4 | In vivo antitumor efficacy of stERAP in OS xenograft mice

We next investigated the in vivo antitumor effect of stERAP in nude mice bearing ectopic HOS cell OS xenografts. Because HOS cell line is available for in vivo xenograft mouse experiments, but MG-63 and Saos-2 cell lines are not due to their low xenotransplantability into nude mice as reported previously,¹³ we used only HOS cells for in vivo experiments. When the tumors reached approximately 100 mm³ after injection of HOS cells into the dorsal region, 1 mg/kg stERAP or vehicle (PBS) was intravenously administered weekly for 4 weeks. Treatment with stERAP caused significant inhibition of tumor growth without body weight loss (Figure 4A,B), as reported previously.¹¹ Notably, tumors were completely ablated in two of the five mice treated with stERAP by 21 days after treatment. To

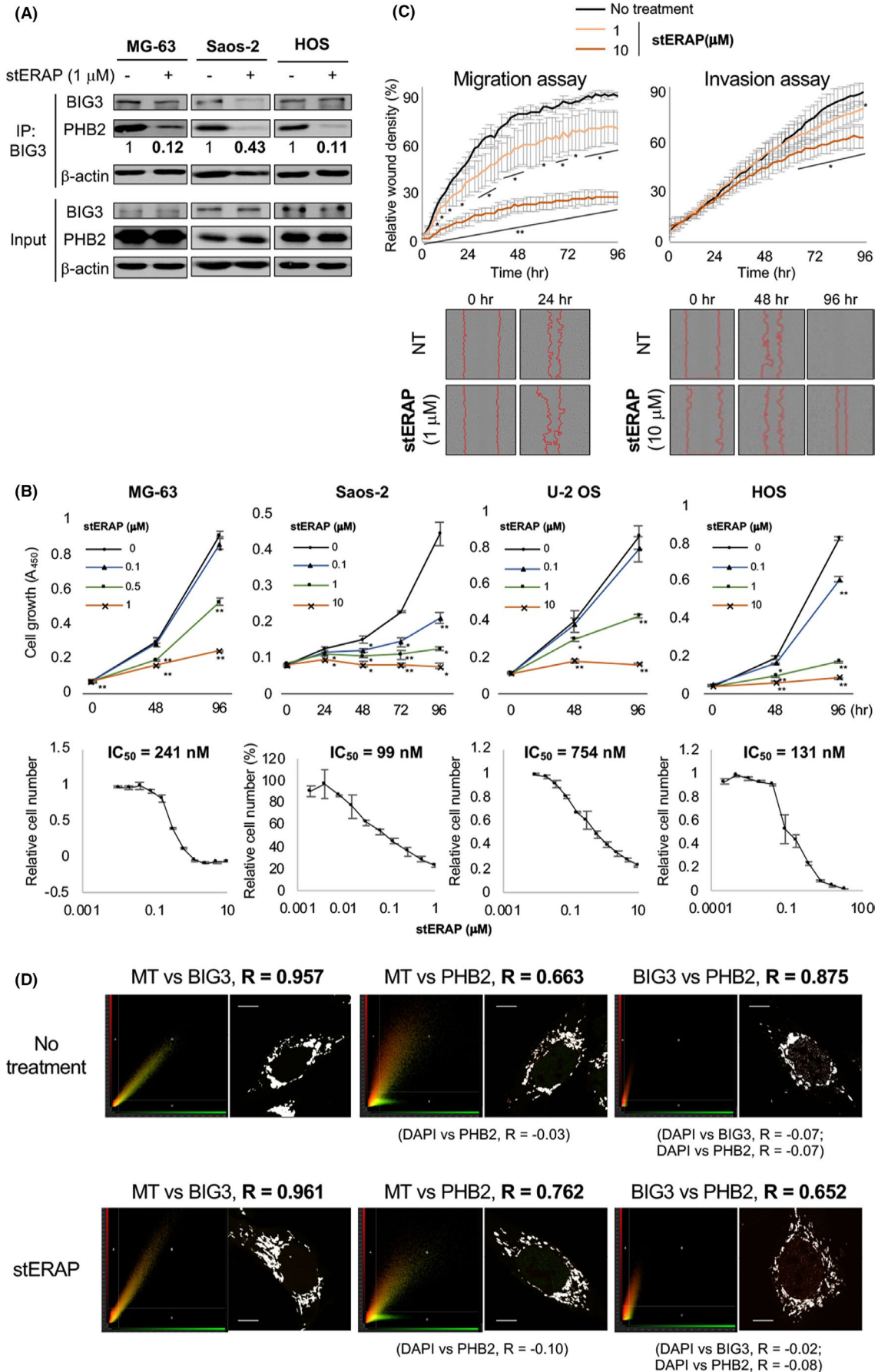


FIGURE 2 Inhibition of mitochondrial brefeldin A-inhibited guanine nucleotide exchange protein 3–prohibitin 2 (BIG3-PHB2) complex formation suppressed the proliferation, migration, and invasion of osteosarcoma (OS) cells. **A**, Inhibitory effect of stapled estrogen receptor alpha activity regulator synthetic peptide (stERAP) treatment on BIG3-PHB2 complex formation in MG-63, Saos-2, and HOS cells. The protein expression levels of PHB2 and BIG3 were determined through densitometric quantification by using an Image Reader LAS-3000 Mini,⁷ and the expression level of PHB2 was then normalized to the corresponding expression level of BIG3 in each cell line. **B**, stERAP suppressed cell proliferation (upper panels) in a dose-dependent manner, as determined by a WST-8 assay with IC₅₀ calculation (lower panels). A₄₅₀, absorbance at 450 nm. Two independent experiments were performed. **C**, Real-time quantitative live-cell imaging analysis showed that stERAP suppressed the migration (left panel) and invasion (right panel) of Saos-2 cells in a dose-dependent manner. NT, no treatment. The lower panels indicate the representative microscopic observations in migration and invasion assays. Two independent experiments were performed. **D**, Colocalization analyses using MG-63 cells treated with/without stERAP for comparison of each pair of fluorescence signals in the multicolor immunostaining images. The white area shows the overlap of each signal. Scale bar, 10 μm. (Upper panels) The Pearson correlation coefficients (R) were shown for MitoTracker (MT) vs BIG3 (left), MT vs PHB2 (middle), and BIG3 vs PHB2 (right), respectively. In the same images, R was -0.07 for DAPI vs BIG3 and -0.03/-0.07 for DAPI vs PHB2, indicating almost no colocalization. (Lower panels) R was 0.961, 0.762, and 0.652 for MT vs BIG3 (left), MT vs PHB2 (middle), and BIG3 vs PHB2 (right), respectively. In the same images, R was -0.02 for DAPI vs BIG3 and -0.10/-0.08 for DAPI vs PHB2, indicating almost no colocalization. Two independent experiments were performed

clarify the mechanisms underlying the *in vivo* antitumor effect of stERAP, we examined the effect of stERAP on BIG3-PHB2 complex formation in tumors resected 35 days after cell transplantation. Coimmunoprecipitation experiments with these tumor tissues indicated that stERAP treatment effectively inhibited the endogenous BIG3-PHB2 interaction (Figure 4C). In addition, treatment of tumors with stERAP led to markedly elevated levels of cleaved PARP (Figure 4D), recapitulating the apoptosis induction as well as PARP cleavage observed *in vitro* (Figure 3D). Moreover, we next conducted an M30 cytodeath staining experiment,¹⁴ which detects early apoptotic events, in stERAP-treated tumor tissues from mice xenograft. The results show that the expression frequency of M30 was significantly higher in the stERAP-treated mice than that in the no-treatment group (Figure 4E). Taken together, these findings suggested that stERAP treatment resulted in sustained inhibition of BIG3-PHB2 complex formation in tumors, thereby inducing PARP cleavage and apoptosis and allowing suppression of OS growth *in vivo*.

3.5 | Impacts of BIG3-PHB2 complex disruption on mitochondrial functions in cancer cells

To clarify the biological functions of the mitochondrial BIG3-PHB2 complex, we conducted 2DICAL and functional annotation analysis using the Database for Annotation, Visualization and Integrated Discovery (DAVID) to identify the differential expression of proteins and pathways in MG-63 cells treated with stERAP. These analyses identified several mitochondrial gene ontology (GO) terms and clusters, including respiratory electron transport chain/mitochondrion, oxidative phosphorylation/mitochondrial protein complex, mitochondrion, peptide metabolic process/(mitochondrial) translation, and oxidation-reduction process/mitochondrial protein complex, that were significantly changed at either 24 or 48 hours after stERAP treatment compared with control treatment (Figure S7A; Table S1 and S2). Furthermore, to identify the mitochondrial characteristics of stERAP-treated OS cells, Gene Set Enrichment Analysis

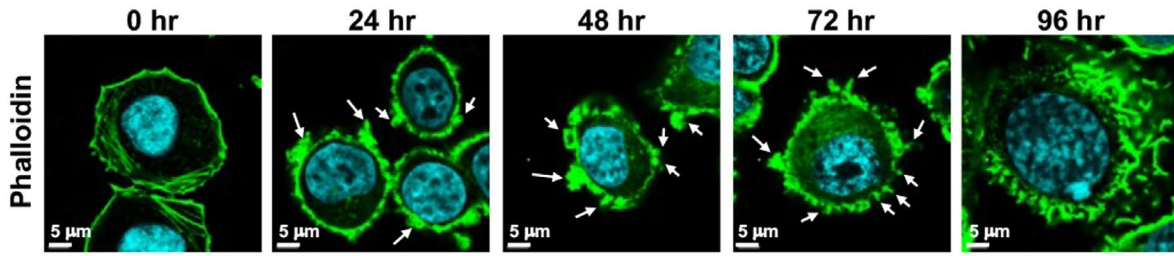
was performed based on the C5.CC (GO, cellular component) and C5.BP (GO, biological processes) curated gene sets as described in the “Methods” section. Notably, genes related to the terms inner mitochondrial membrane organization (normalized enrichment score [NES] = -1.44, *P* = .000) and mitochondrial membrane part (NES = -1.43, *P* = .000) were significantly downregulated at 24 hours after stERAP treatment, and genes related to the term regulation of mitochondrial membrane potential (NES = -1.51, *P* = .000) were significantly downregulated at 48 hours after stERAP treatment (Figure S7B). These findings suggest that disruption of the BIG3-PHB2 complex might lead to dysregulation of mitochondrial membrane-related functions in OS cells.

3.6 | Inhibition of mitochondrial BIG3-PHB2 complex formation induces activation of the PARP-AIF-dependent pathway

Pathway analysis with DAVID revealed that genes in the DNA repair pathway GO term were significantly upregulated after 24 hours of stERAP treatment (Figure S7A). Moreover, unexpectedly, stERAP treatment led to significant upregulation of full-length PARP protein expression in MG-63 cells at 48 hours (Figure 3D). Therefore, we hypothesized that disruption of the BIG3-PHB2 complex by stERAP treatment leads to apoptosis mediated by the mitochondrial protein AIF. First, we confirmed the stERAP-mediated upregulation of PARP-1 in MG-63 cells at the mRNA and protein levels by qRT-PCR (Figure 5A) and Western blotting (Figure 5B), respectively. Notably, AIF was cleaved from 24 to 48 hours after stERAP treatment (Figure 5B), while cytochrome *c* was not yet released from mitochondria into the cytoplasm at 48 hours after stERAP treatment due to the early phase of apoptosis (Figure 5C). Moreover, a small fraction of mitochondrial PARP interacted with mitochondrial BIG3 in OS cells (Figure 5D and 5E). These findings suggest the possibility that inhibition of BIG3-PHB2 complex formation might activate the PARP-AIF-dependent pathway via activation of mitochondrial PARP in OS cells.

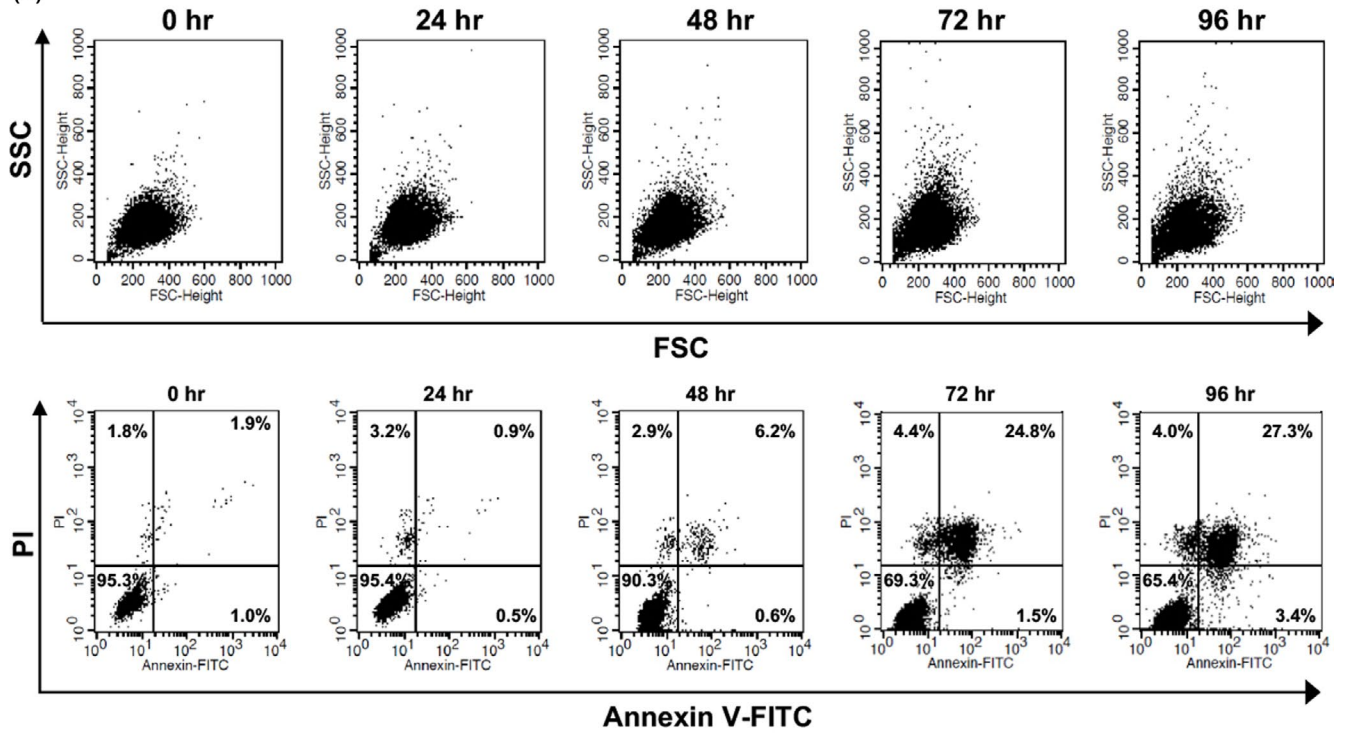
(A)

1 μ M stERAP treatment



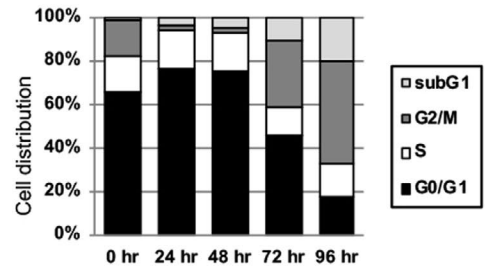
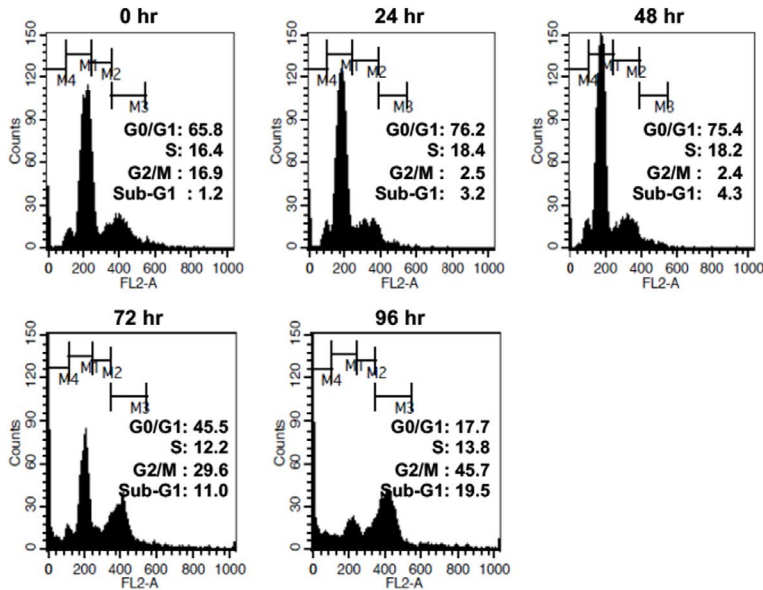
(B)

1 μ M stERAP



(C)

1 μ M stERAP



(D)

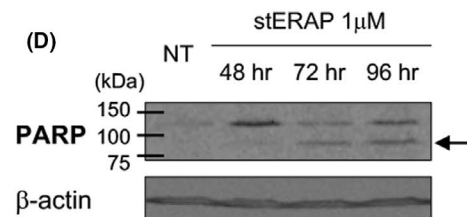


FIGURE 3 Stapled estrogen receptor alpha activity regulator synthetic peptide (stERAP) treatment induced cell cycle arrest and subsequent cell death in MG-63 cells. **A**, Phalloidin staining of MG63 cells treated with stERAP for 0, 24, 48, 72, and 96 h. Treatment with stERAP induced morphological alterations, such as membrane blebbing or the formation of some apoptotic body-like small vesicles (arrows). **B**, Apoptosis analysis by annexin V/PI double-staining of MG63 cells treated with 1 μ M stERAP for 0, 24, 48, 72, and 96 h. **C**, Flow cytometric analyses showing the effect of stERAP on the cell cycle in MG63 cells. **D**, Western blot analysis showed cleaved PARP, indicated by the arrow, in whole-cell lysates of cells treated with/without stERAP. Full-length PARP expression at 48 h was considerably upregulated approximately 3.8-fold compared with that in untreated cells (NT), as determined by densitometry. Two independent experiments were performed

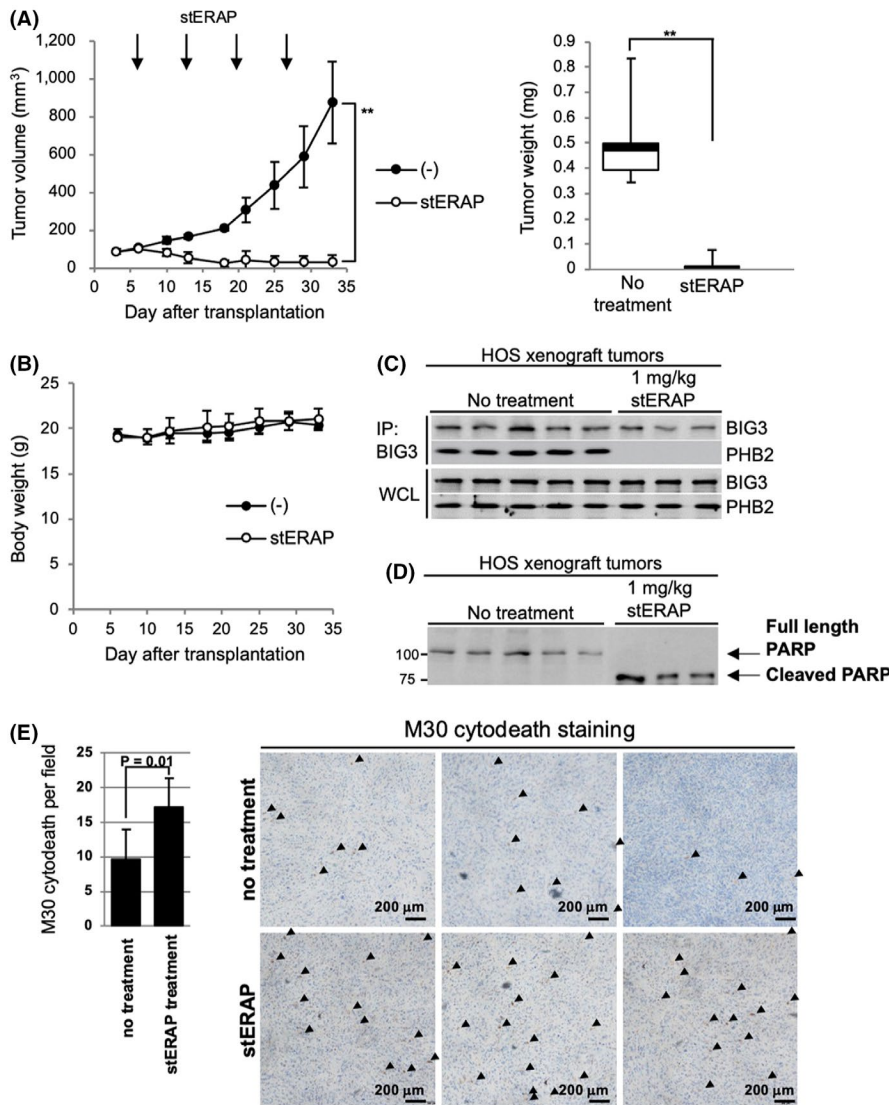


FIGURE 4 Stapled estrogen receptor alpha activity regulator synthetic peptide (stERAP) exhibited in vivo antitumor efficacy in xenograft models of human osteosarcoma (OS). **A**, Tumor growth was assessed after weekly intravenous injection of stERAP into mice bearing ectopic OS xenografts. The tumor volumes (left) and tumor weights (right) are presented as the mean \pm SD of each group (n = 5). ***P* < .001 via two-tailed Student's *t*-tests. **B**, Body weights of OS xenograft-bearing mice treated with weekly intravenous administration of stERAP. The body weights are presented as the mean \pm SD of each group (n = 5). **C**, **D**, Immunoblot analysis of the inhibition of the brefeldin A-inhibited guanine nucleotide exchange protein 3-prohibitin 2 (BIG3-PHB2) interaction (**C**) and PARP cleavage (**D**) in tumors treated with weekly intravenous administration of stERAP. **E**, Representative immunohistochemical staining for M30, a maker of apoptosis, tumors at day 35. The expression frequency of M30, indicated by the arrow in right panels, was significantly higher in the stERAP-treated mice than that in the no-treatment group

4 | DISCUSSION

The present study revealed the first evidence that BIG3 forms a complex with PHB2 in mitochondria in OS cells, in contrast to its cytoplasmic localization in estrogen-dependent breast cancer cells^{6-8,10,11} and that this mitochondrial complex plays important roles in the malignant phenotype of OS. Disruption of the BIG3-PHB2 complex via either knockdown of BIG3 or treatment with the BIG3-PHB2 interaction inhibitory peptide stERAP resulted in suppression of OS cell proliferation, migration, and invasion, finally leading to apoptosis. Notably, the mitochondrial localization of

the BIG3-PHB2 complex in OS cells was not changed even when the BIG3-PHB2 interaction was inhibited by stERAP (Figure 2D; Figure S3). However, in breast cancer cells, PHB2 released from BIG3 by stERAP translocates into the nucleus, thereby functioning as a corepressor of ER α transcriptional activity.⁶⁻¹¹ Considering the subcellular localization of PHB2 described in previous reports, PHB2 forms a complex with PHB1 and is localized either within the inner membrane or extending into the intermembrane space of mitochondria.¹⁷ Accordingly, these findings suggest that the BIG3-PHB2 complex plays distinct crucial roles in tumorigenesis and progression at each subcellular location, although the determinants

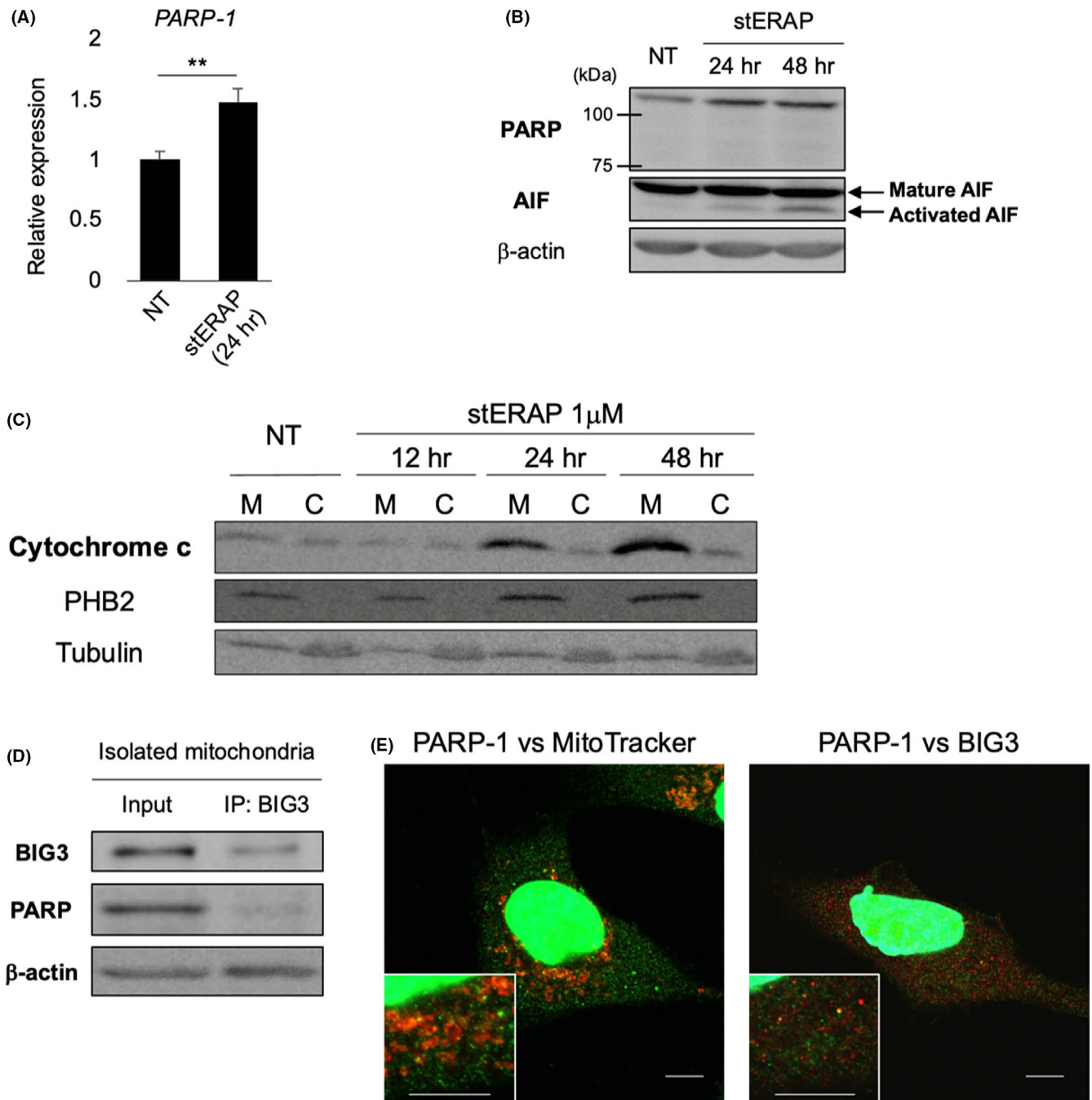


FIGURE 5 Disruption of the brefeldin A-inhibited guanine nucleotide exchange protein 3–prohibitin 2 (BIG3-PHB2) complex induces mitochondrial dysfunction. A, qRT-PCR showed upregulated *PARP-1* expression after stapled estrogen receptor alpha activity regulator synthetic peptide (stERAP) treatment at 24 h compared with no treatment (NT). Two independent experiments were performed. B, Western blot analysis showed upregulated PARP at 24 and 48 h and activated apoptosis-inducing factor (AIF) in a time-dependent manner. Two independent experiments were performed. C, Western blot analysis showed that most cytochrome c was localized in mitochondria in the MG-63 cell lysate even under stERAP treatment for 12, 24, and 48 h. M, mitochondria, C, cytosol. Two independent experiments were performed. D, Immunoprecipitation-immunoblot analyses showed that BIG3 interacted with endogenous mitochondrial PARP. IP, immunoprecipitated sample in MG-63 cells. E, A small fraction of PARP-1 (green) was merged with MitoTracker (red, left) and BIG3 (red, right) by immunocytochemistry and multicolor staining using MG-63 cells. Scale bar, 10 μm

that control the distinct subcellular localization of the BIG3-PHB2 complex must be identified.

Intriguingly, we found that stERAP treatment induced G2/M arrest and sequential apoptotic events. Previous studies reported that

a DNA targeting antitumor intercalator, C-1311, and DNA topoisomerase II inhibitor, F14512, induced G2/M arrest followed by enlarged cells and apoptosis in human leukemia or melanoma cells.^{18,19} Similarly, stERAP treatment resulted in a significant time-dependent

increase in cell size in OS cells (Figure S8A). Further analyses of the mechanism of stERAP's effect on enlarged cells followed by apoptosis in OS cells in more detail will be necessary.

More importantly, PARP protein expression was obviously up-regulated in stERAP-treated cells compared with nontreated OS cells (Figure 3D), and a small fraction of mitochondrial PARP interacted with mitochondrial BIG3 in OS cells (Figure 5D and 5E). Moreover, stERAP treatment led to activation of the PARP-1/AIF-dependent pathway in OS cells (Figure 5B). Accordingly, our findings suggest that the BIG3-PHB2 complex might regulate the mitochondrial PARP-1/AIF apoptotic pathway via direct binding to mitochondrial PARP-1 in OS cells. By contrast, disruption of mitochondrial BIG3-PHB2 complex formation led to mitochondrial failure and thereby to cell morphological changes such as apoptotic body formation (Figure 3; Figure S5; Figure S6), finally resulting in PARP1/AIF-dependent apoptosis. Moreover, the characteristic phenotypes of this cell death, such as indistinct membrane blebbing and lack of shrinkage, seemed to diverge from the principle of apoptosis.²⁰ Szczensny B et al reported that PARP-1 is localized in mitochondria and has negative effects on mitochondria-specific functions that suppress biogenesis, including decreases in the mitochondrial DNA copy number and membrane potential, unlike the well-known nuclear PARP-1.²¹ Moreover, knockdown of mitofilin, which, like PHB2, is a mitochondrial inner membrane protein, promotes apoptosis via AIF-PARP pathway activation.²² Collectively, these findings possibly indicate that disruption of mitochondrial BIG3-PHB2 complex formation in OS cells might cause more severe effects than disruption of cytoplasmic BIG3-PHB2 complex formation.

Furthermore, we demonstrated the disruption of the BIG3-PHB2 complex results in a reduced migratory and invasive capacity, which are important aspects of oncogenic progression leading to lethal metastasis, in OS cells. Interestingly and unexpectedly, stERAP treatment resulted in drastically increased coimmunoprecipitation of BIG3 and β -actin in MG-63 cells (Figure S8B). Notably, we demonstrated that stERAP suppressed the migration and invasion of OS cells (Figure 2C). Actin filaments are the principal cytoskeletal components related to motility and are especially essential in protrusive structures such as filopodia and lamellipodia.²³ In addition, actin dynamics are important for the control of mitochondrial function through the mitochondrial membrane protein complex.²⁴ Accordingly, mitochondrial dysfunction induced by stERAP treatment is thought to involve cell migration and invasion due to dysregulation of actin filaments, as argued in recent studies.²⁵ However, further studies to clarify this possibility are required.

Most importantly, from a therapeutic perspective, we demonstrated that the efficacy of stERAP in OS cells both in vitro and in vivo was equal to or more potent than that in ER α -positive breast cancer cells, as shown by comparison of the IC₅₀ values and growth curve obtained in the current study (Figure 2B; Figure 4A) with those in previous reports.¹¹

In conclusion, our findings show that the BIG3-PHB2 complex in mitochondria plays critical roles in OS tumor growth and development and that its disruption may result in apoptotic cell death

and decreases in the migration and invasion abilities of OS cells. The novel therapeutic strategy of inhibiting the BIG3-PHB2 protein-protein interaction might be promising in OS.

ACKNOWLEDGMENTS

We are grateful to Ms Hitomi Kawakami and Ms Hinako Koseki (Division of Genome Medicine, Tokushima University) for providing excellent technical support and to Toshihiko Nishisho (Department of Orthopedics, Tokushima University Graduate School) for providing valuable advice. We thank Prof Koichi Matsuda (University of Tokyo) for providing valuable suggestion on using Saos 2 and U2OS cell lines. This study was supported by Grants-in-Aid for Scientific Research on Innovative Area (JP17H06419); Grants-in-Aid for Scientific Research (B) (JP16H05153), (C) (JP18K07200), and (A) (JP20H00543) from the MEXT of Japan; and by the Project for Cancer Research and Therapeutic Evolution (P-CREATE) from AMED (19191248), Japan. The present study was also supported by the Joint Usage and Joint Research Programs, the Institute of Advanced Medical Sciences, Tokushima University, and the Research Cluster Program of Tokushima University.

CONFLICT OF INTEREST

T. Katagiri is an external board member and stockholder of Onco Therapy Science, Inc. The remaining authors have no potential conflict of interest.

ORCID

Toyomasa Katagiri  <https://orcid.org/0000-0001-5086-7444>

REFERENCES

- Smeland S, Bielack SS, Whelan J, et al. Survival and prognosis with osteosarcoma: outcomes in more than 2000 patients in the EURAMOS-1 (European and American Osteosarcoma Study) cohort. *Eur J Cancer*. 2019;109:36-50.
- Meazza C, Bastoni S, Scanagatta P. What is the best clinical approach to recurrent/refractory osteosarcoma? *Expert Rev Anticancer Ther*. 2020;20:415-428.
- Ritter J, Bielack Ss. Osteosarcoma. *Annals of Oncology*. 2010;21:vii320-vii325. <https://doi.org/10.1093/annonc/mdq276>
- Zhang Y, Yang J, Zhao N, et al. Progress in the chemotherapeutic treatment of osteosarcoma. *Oncol Lett*. 2018;16:6228-6237.
- Zhao J, Dean DC, Hornicek FJ, et al. Emerging next-generation sequencing-based discoveries for targeted osteosarcoma therapy. *Cancer Lett*. 2020;474:158-167.
- Kim JW, Akiyama M, Park JH, et al. Activation of an estrogen/estrogen receptor signaling by BIG3 through its inhibitory effect on nuclear transport of PHB2/REA in breast cancer. *Cancer Sci*. 2009;100:1468-1478.
- Yoshimaru T, Ono M, Bando Y, et al. A-kinase anchoring protein BIG3 coordinates oestrogen signalling in breast cancer cells. *Nat Commun*. 2017;8:15427.
- Yoshimaru T, Komatsu M, Matsuo T, et al. Targeting BIG3-PHB2 interaction to overcome tamoxifen resistance in breast cancer cells. *Nat Commun*. 2013;4:2443.
- Chen YA, Murakami Y, Ahmad S, et al. Brefeldin A-inhibited guanine nucleotide-exchange protein 3 (BIG3) is predicted to interact with its partner through an ARM-type alpha-helical structure. *BMC Res Notes*. 2014;7:435.

10. Yoshimaru T, Komatsu M, Miyoshi Y, et al. Therapeutic advances in BIG3-PHB2 inhibition targeting the crosstalk between estrogen and growth factors in breast cancer. *Cancer Sci.* 2015;106:550-558.
11. Yoshimaru T, Aihara K, Komatsu M, et al. Stapled BIG3 helical peptide ERAP potentiates anti-tumour activity for breast cancer therapeutics. *Sci Rep.* 2017;7:1821.
12. Scott MC, Temiz NA, Sarver AE, et al. Comparative Transcriptome Analysis Quantifies Immune Cell Transcript Levels, Metastatic Progression, and Survival in Osteosarcoma. *Cancer Res.* 2018;78:326-337.
13. Lauvrak SU, Munthe E, Kresse SH, et al. Functional characterisation of osteosarcoma cell lines and identification of mRNAs and miRNAs associated with aggressive cancer phenotypes. *Br J Cancer.* 2013;109:2228-2236.
14. Tajima H, Ohta T, Kitagawa H, et al. Neoadjuvant chemotherapy with gemcitabine for pancreatic cancer increases in situ expression of the apoptosis marker M30 and stem cell marker CD44. *Oncol Lett.* 2012;3:1186-1190.
15. Yuan Y & Li Y Gene expression profiling in Osteosarcomas. NCBI GEO. Available from: <https://www.ncbi.nlm.nih.gov/geo/query/acc.cgi?acc=GSE126209>
16. Coleman ML, Sahai EA, Yeo M, Bosch M, Dewar A, Olson MF. Membrane blebbing during apoptosis results from caspase-mediated activation of ROCK I. *Nat Cell Biol.* 2001;3:339-345.
17. Yoshinaka T, Kosako H, Yoshizumi T, et al. Structural Basis of Mitochondrial Scaffolds by Prohibitin Complexes: Insight into a Role of the Coiled-Coil Region. *iScience.* 2019;19:1065-1078.
18. Skwarska A, Augustin E, Konopa J. Sequential induction of mitotic catastrophe followed by apoptosis in human leukemia MOLT4 cells by imidazoacridinone C-1311. *Apoptosis.* 2007;12:2245-2257.
19. Ballot C, Jendoubi M, Kluza J. Regulation by survivin of cancer cell death induced by F14512, a polyamine-containing inhibitor of DNA topoisomerase II. *Apoptosis.* 2012;17:364-376.
20. Maeno E, Ishizaki Y, Kanaseki T, et al. Normotonic cell shrinkage because of disordered volume regulation is an early prerequisite to apoptosis. *Proc Natl Acad Sci U S A.* 2000;97:9487-9492.
21. Szczesny B, Brunyanski A, Olah G, et al. Opposing roles of mitochondrial and nuclear PARP1 in the regulation of mitochondrial and nuclear DNA integrity: implications for the regulation of mitochondrial function. *Nucleic Acids Res.* 2014;42:13161-13173.
22. Madungwe NB, Feng Y, Lie M, et al. Mitochondrial inner membrane protein (mitofilin) knockdown induces cell death by apoptosis via an AIF-PARP-dependent mechanism and cell cycle arrest. *Am J Physiol Cell Physiol.* 2018;315:C28-C43.
23. Mitchison TJ, Cramer LP. Actin-based cell motility and cell locomotion. *Cell.* 1996;84:371-379.
24. Hoffmann L, Rust MB, Culmsee C. Actin(g) on mitochondria - a role for cofilin1 in neuronal cell death pathways. *Biol Chem.* 2019;400:1089-1097.
25. Denisenko TV, Gorbunova AS, Zhivotovsky B. Mitochondrial Involvement in Migration, Invasion and Metastasis. *Front Cell Dev Biol.* 2019;7:355.

SUPPORTING INFORMATION

Additional supporting information may be found online in the Supporting Information section.

How to cite this article: Toki S, Yoshimaru T, Matsushita Y, et al. The survival and proliferation of osteosarcoma cells are dependent on the mitochondrial BIG3-PHB2 complex formation. *Cancer Sci.* 2021;112:4208-4219. <https://doi.org/10.1111/cas.15099>